A CORRELATION BETWEEN STAR FORMATION RATE AND AVERAGE BLACK HOLE ACCRETION IN STAR-FORMING GALAXIES

Chien-Ting J. Chen[1], Ryan C. Hickox[1], Stacey Alberts[2], Mark Brodwin[3], Christine Jones[4], Stephen S. Murray[5],
David M. Alexander[6], Roberto J. Assef[7,11], Michael J. I. Brown[8], Arjun Dey[9], William R. Forman[4], Varoujan Gorjian[7],
Andrew D. Goulding[4], Emeric Le Floc'h[10], Buell T. Jannuzi[9], James R. Mullaney[6,10], and Alexandra Pope[2]

[1] Department of Physics and Astronomy, Dartmouth College, 6127 Wilder Laboratory, Hanover, NH 03755, USA; ctchen@dartmouth.edu
[2] Department of Astronomy, University of Massachusetts, Amherst, MA 01003, USA
[3] Department of Physics and Astronomy, University of Missouri, 5110 Rockhill Road, Kansas City, MO 64110, USA
[4] Harvard-Smithsonian Center for Astrophysics, 60 Garden Street, Cambridge, MA 02138, USA
[5] Department of Physics and Astronomy, The Johns Hopkins University, 3400 N. Charles Street, Baltimore, MD 21218, USA
[6] Department of Physics, Durham University, South Road, Durham DH1 3LE, UK
[7] Jet Propulsion Laboratory, California Institute of Technology, Pasadena, CA 91109, USA
[8] School of Physics, Monash University, Clayton 3800, Victoria, Australia
[9] National Optical Astronomy Observatory, Tucson, AZ 85726, USA
[10] Laboratoire AIM-Paris-Saclay, CEA/DSM/Irfu-CNRS-Université Paris Diderot, CE-Saclay, pt courrier 131, F-91191 Gif-sur-Yvette, France

ABSTRACT

We present a measurement of the average supermassive black hole accretion rate (BHAR) as a function of the star formation rate (SFR) for galaxies in the redshift range $0.25 < z < 0.8$. We study a sample of 1767 far-IR-selected star-forming galaxies in the 9 deg^2 Boötes multi-wavelength survey field. The SFR is estimated using 250 μm observations from the *Herschel Space Observatory*, for which the contribution from the active galactic nucleus (AGN) is minimal. In this sample, 121 AGNs are directly identified using X-ray or mid-IR selection criteria. We combined these detected AGNs and an X-ray stacking analysis for undetected sources to study the *average* BHAR for all of the star-forming galaxies in our sample. We find an almost linear relation between the average BHAR (in $M_\odot$ yr^{-1}) and the SFR (in $M_\odot$ yr^{-1}) for galaxies across a wide SFR range $0.85 < \log \mathrm{SFR} < 2.56 : \log \mathrm{BHAR} = (-3.72 \pm 0.52) + (1.05 \pm 0.33) \log \mathrm{SFR}$. This global correlation between SFR and average BHAR is consistent with a simple picture in which SFR and AGN activity are tightly linked over galaxy evolution timescales.

Key words: galaxies: active – galaxies: evolution – galaxies: starburst – infrared: galaxies – X-rays: galaxies

Online-only material: color figures

1. INTRODUCTION

Observational studies have shown that the mass of galactic bulges is tightly correlated with the mass of their central supermassive black holes (SMBHs; e.g., Magorrian et al. 1998; Ferrarese & Merritt 2000; Gebhardt et al. 2000; Marconi et al. 2004), and that the black hole accretion rate (BHAR) density and star formation rate (SFR) density both peak at a similar redshift before declining to the present day (e.g., Hopkins & Beacom 2006; Rodighiero et al. 2010; Silverman et al. 2009; Aird et al. 2010). Together, these results may imply parallel evolutionary paths for the growth of SMBHs and the stellar mass of their host galaxies. However, the physical mechanisms that drive this apparent link between SF and BH growth over a wide variety of galaxies are still poorly understood.

Active SMBH accretion (i.e., active galactic nucleus, AGN) and galactic star formation (SF) both require a supply of gas. Thus, the clues of uncovering the connection between their growth may lie in the gas fueling mechanisms that supply both galactic SF and AGNs. Recent studies have observed the existence of two different modes of SF: the quiescent "main sequence" SF and starbursts (Genzel et al. 2010; Elbaz et al. 2011). The first mode can be fueled by continuous gas inflow (Kawakatu & Wada 2008; Dekel et al. 2009; Ciotti et al. 2010) and the second mode is postulated to be triggered by gas-rich major mergers (e.g., Hopkins & Hernquist 2009a; Veilleux et al.

2009). However, it is still not clear whether these processes also drive the growth of SMBHs, or whether SMBH growth would scale similarly with galactic SF in different SF modes, since the dynamical scales of the gas inflows that induce galactic SF and SMBH accretion are vastly different (see Alexander & Hickox 2012, for a review).

A number of studies have investigated the link between SFR and BHAR. For high-luminosity AGNs, an increase in the average SFR as a function of BHAR has been observed (e.g., Lutz et al. 2008; Serjeant & Hatziminaoglou 2009; Serjeant et al. 2010; Mor et al. 2012), while other studies have also found weak or inverted connections (Page et al. 2012; Harrison et al. 2012). Studies with inclusions of lower luminosity AGNs further suggest that the evolutionary link between SMBHs and their host galaxies only exists in high-luminosity AGNs that are possibly triggered by mergers, and there is little or no correlation at lower luminosities (e.g., Shao et al. 2010; Lutz et al. 2010; Rosario et al. 2012; Rovilos et al. 2012). On the contrary, the study of the *average* BHAR of star-forming galaxies implies that the galaxy and SMBH growth rates may be strongly connected when averaging over the whole population of star-forming galaxies (Rafferty et al. 2011; Mullaney et al. 2012b). Thus, whether BH growth follows SF in all galaxies, or only in the most powerful systems, remains a matter of debate.

The apparently contradictory results may be attributed to the difference in the characteristic timescales of SF and BH accretion. Theoretical studies of SMBH accretion with feedback imply that the SMBH accretion rate can vary by more than five

---
[11] NASA Postdoctoral Program Fellow.

orders of magnitudes on a timescale of less than 1 Myr (Novak et al. 2011). Observational studies of AGNs also suggest that the observed AGN Eddington ratios range from $<10^{-4}$ to ~1 for AGN hosts with similar properties (Hickox et al. 2009; Hopkins & Hernquist 2009b; Aird et al. 2012; Bongiorno et al. 2013). Recent evidence for rapid AGN variability over a large dynamic range in accretion rate comes from the discovery of giant ionized clouds around galaxies with little or no current AGN activity (Schawinski et al. 2010), indicating a drop in AGN luminosity by $>10^5$ in $<10^5$ yr (Keel et al. 2012a, 2012b). There is also observational evidence in the X-ray Fe Kα echoes from the quiescent SMBH in the center of the Milky Way, suggesting it might have been a low-luminosity AGN a few hundred years ago (e.g., Revnivtsev et al. 2004; Ponti et al. 2010; Nobukawa et al. 2011). In contrast to the accretion rate of an individual SMBH, the galactic SFR is relatively stable. Even short-lived starbursts last ~100 Myr (e.g., Wong 2009; Ostriker et al. 2010; Hickox et al. 2012), which is still much longer than the timescale of AGN variability.

The key quantity to study may therefore be the *average* AGN luminosity of a population, which thus smoothes over the variations of individual sources. Recent studies (e.g., Hopkins & Hernquist 2009b; Aird et al. 2012; Bongiorno et al. 2013) have discovered that the shape of the distribution function of the AGN Eddington ratio is independent of the properties of the hosting galaxies, thus the average AGN luminosity is a reliable tool to study the long-term BHAR in any sample of galaxies.

Measuring SFRs in AGN host galaxies can be challenging because of obscuring dust and contamination from AGNs. Detailed spectral template fitting is required to disentangle AGN and star-forming activities in optical or mid-IR observations (e.g., Kauffmann et al. 2003; Pope et al. 2008). In contrast, at far-IR wavelengths, at which the thermal emission from the cold dust peaks, the AGN contaminates the least (e.g., Netzer et al. 2007; Hatziminaoglou et al. 2010; Mullaney et al. 2011). Therefore, the 250 μm filter on the Spectral and Photometric Imaging Receiver (SPIRE; Griffin et al. 2010) on board the *Herschel Space Observatory* provides an excellent tool to probe the dust-enshrouded SF activities of galaxies hosting AGNs at $z < 1$.

For this paper, we utilized 250 μm *Herschel* SPIRE observations to constrain the SFR of a sample of star-forming galaxies with spectroscopic redshift measurements from the AGN and Galaxy Evolution Survey (AGES; Kochanek et al. 2012). We also supplemented the AGES redshift measurements with photometric redshifts from Spitzer Deep Wide-Field Survey (SDWFS; Ashby et al. 2009) and the *Spitzer* IRAC (Infrared Array Camera) Shallow Survey (ISS; Brodwin et al. 2006). We focused on studying the correlations between the SFR and the BHAR of galaxies in a redshift range of $0.25 < z < 0.8$. To determine the connection between the SF activity and the *average* SMBH accretion rate, we measure AGN luminosities using a combination of X-ray and mid-IR observations from the *Chandra* XBoötes (Murray et al. 2005; Kenter et al. 2005) survey, the *Spitzer* ISS, and SDWFS catalogs. For galaxies without identified AGNs, we employed an X-ray stacking analysis.

This paper is organized as follows: in Section 2, we describe the multi-wavelength data and the properties of the galaxy and AGN samples, along with the methods we adopted to obtain their SFR and average X-ray luminosity. The results of our SFR and SMBH accretion rate analysis is presented in Section 3, and we provide a discussion and a summary in Section 4. Throughout the paper, we assume a ΛCDM cosmology with $\Omega_m = 0.3$

and $\Omega_\Lambda = 0.7$. For direct comparison with other works, we assume $H_0 = 70$ km s^{-1} Mpc^{-1}; however, our conclusions are insensitive to the exact choice of cosmological parameters.

2. DATA AND SAMPLE SELECTION

2.1. Redshifts

We selected *Herschel*-observed star-forming galaxies in the 9 deg^2 Boötes field covered by the NOAO Deep Wide-Field Survey (NDWFS; Jannuzi & Dey 1999) to measure the correlation between the SFR and the BHAR in star-forming galaxies. For the redshifts in this study, we primarily used the spectroscopic redshifts in the range $0.25 < z < 0.8$ from the AGES Data Release 2 (Kochanek et al. 2012), which covers 7.7 deg^2 of NDWFS. To maximize the completeness for our sample of IR-selected SF galaxies, we also supplemented the data with photometric redshifts measured using the data from the 8.5 deg^2 *Spitzer* ISS (Eisenhardt et al. 2004; Stern et al. 2005) and the 10 deg^2 SDWFS (Ashby et al. 2009). The photometric redshifts were derived using all four IRAC bands (3.6, 4.5, 5.8, and 8 μm) in ISS and SDWFS, with the algorithm developed by Brodwin et al. (2006, B06 hereafter). We limited our photometric redshifts to the same redshift range as the spectroscopic redshifts, in which the accuracy of the photometric redshifts is $\sigma = 0.06(1 + z)$ for 95% of galaxies and $\sigma = 0.12(1 + z)$ for 95% of AGNs (Brodwin et al. 2006).

2.2. Infrared Data

In addition to the IRAC observations, we also used far-IR and mid-IR data from *Herschel* and the Multiband Imaging Photometer (MIPS) on board *Spitzer*, respectively. The far-IR data in this work are based on the publicly available *Herschel* SPIRE 250 μm observations from the Herschel Multi-tiered Extragalactic Survey (HerMES; Oliver et al. 2012). We re-reduced and mosaiced the Boötes SPIRE observations (S. Alberts et al., in preparation), which include a deep ~2 deg^2 inner region in the center of the field and a shallower ~8.5 deg^2 outer region. We specifically focused on removing stripping, astrometry offsets, and glitches missed by the standard pipeline reduction. We also convolved the raw maps with a matched filter (see Chapin et al. 2011), which aided in source extraction by lowering the overall noise and de-blending sources. From this, we generated a matched filter catalog with 21,892 point sources above S/N > 5. Completeness simulations showed that these catalogs are 95% complete in the inner region and 69% complete in the outer regions above a flux limit of 20 mJy. We also found minimal flux boosting for low signal-to-noise ratio (S/N) sources above these flux cutoffs. In addition, we used the 24 μm flux measurements available from the MIPS for *Spitzer* GTO observations (IRS GTO team, J. Houck (PI), and M. Rieke) of the Boötes field as a comparison in the source matching and SFR estimation. This catalog covers an area similar to that of the XBoötes and has 52,089 S/N > 5 sources with flux >0.15 mJy.

2.3. AGN Selection

X-ray observations from the XBoötes survey provide the basis of our measurements of AGN luminosity. The X-ray data in this study are drawn from the 9.3 deg^2 XBoötes survey, which is a mosaic of 126 short (5 ks) *Chandra* ACIS-I images (Murray et al. 2005; Kenter et al. 2005) covering the entire NDWFS. XBoötes contains 2724 X-ray point sources with at least four counts in the AGES survey region. 362 of the 2724 X-ray point

sources are not close to bright stars and matched within 3″.5 to objects with good AGES redshifts at $0.25 < z < 0.8$ (Kenter et al. 2005; Hickox et al. 2009). These X-ray point sources have 0.5–7 keV luminosities of $10^{42} < L_X < 10^{45}$ erg s^{-1}, which are characteristic for moderate- to high-luminosity AGNs and significantly larger than the typical L_X for star-forming galaxies (Ranalli et al. 2003).

To properly estimate the average SMBH accretion rate, it is important to account for obscured AGNs that may have their X-ray flux significantly depressed by photoelectric absorption (e.g., Alexander et al. 2008). We therefore supplemented our AGN sample with AGNs selected with the IRAC color–color selection criteria (Stern et al. 2005) in ISS and SDWFS. These selection criteria has been shown to effectively identify obscured AGNs at moderate redshift (Gorjian et al. 2008; Assef et al. 2010), since mid-IR wavelengths are not as strongly affected by obscuration as the optical or UV (e.g., Lacy et al. 2004; Stern et al. 2005; Donley et al. 2007; Hickox et al. 2007; Goulding & Alexander 2009). In our sample, 1047 AGNs were identified using mid-IR observations (mid-IR AGNs hereafter). Among the 1047 mid-IR AGNs and the 362 X-ray AGNs, 163 of them can be identified as AGNs using both X-ray and mid-IR selection criteria.

2.4. Catalog Matching

Since the large point-spread function (PSF) of SPIRE can lead to spurious matching results, here we discuss our catalog matching procedures. We first matched the entire SPIRE catalog to the 5σ MIPS 24 μm catalog with a matching radius of 5″. We found that ~80% of the SPIRE sources in the coverage of the MIPS catalog have MIPS counterparts within the 5″ radius. While increasing the radius to 10″ can increase the MIPS detection fraction for the SPIRE sources to ~92%, the fraction of SPIRE sources with multiple MIPS counterparts would also increase from 2.9% to 14%; therefore, we chose the 5″ matching radius to avoid spurious matching. These matched sources have a minimum 24 μm flux at least 25% larger than the 0.15 mJy flux limit of the 5σ MIPS 24 μm catalog, which ensures that the matched galaxies are star-forming galaxies that are bright in both mid-IR and far-IR, and that our completeness in 250 μm is not strongly affected by the 24 μm flux limit. Then, we matched the coordinates from the MIPS catalog (with 250 μm counterparts) to the B06 photometric redshift catalog with a matching radius of 2″. We also matched the AGES catalog and the AGES-matched optical positions of X-ray AGNs to the photometric redshift catalog with a matching radius of 1″.

To minimize spurious matches, we tested our matching by offsetting the source positions by 1′ in a random direction. We found that with radius of 1″, our matching between the AGES and B06 catalog yielded <0.1% spurious matches. The radius of the matching between the 250 μm matched MIPS catalog and the B06 catalog is tested to have less than 4% of spurious matches, which greatly reduced the ~25% spurious matching rates obtained when directly matching the SPIRE sources to the B06 catalog.

In our sample, there are 1767 galaxies with both SPIRE and MIPS detections. 1112 of these have spectroscopic redshift measurements, while the remainder have photometric redshifts. 121 of the 1767 sources (~7%) in our sample have been classified as AGNs, in which 34 (~2%) sources are identified as X-ray AGNs using X-ray selection criteria and 107 (~6%) are identified as mid-IR AGNs using mid-IR color–color selection criteria. 20 of the 121 AGNs are identified as both X-ray AGNs
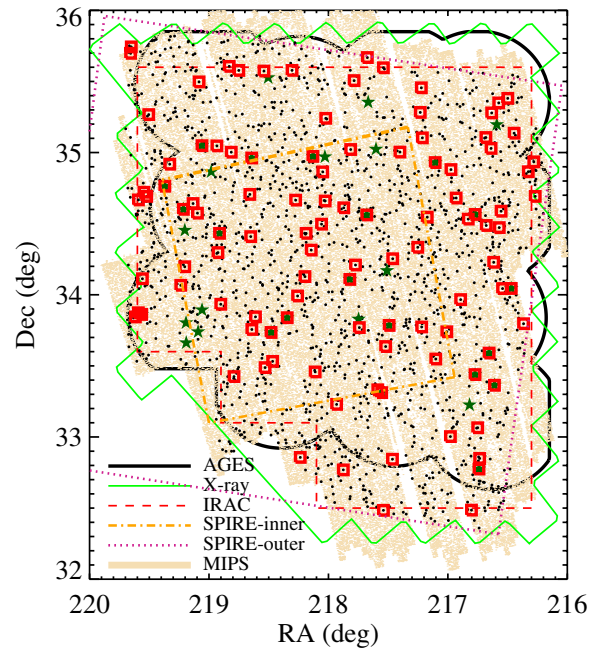

Figure 1. Map of the Boötes survey region, showing approximate areas covered by the AGES, XBoötes (X-ray), IRAC Shallow Survey (mid-IR), and the inner deeper and the outer shallower regions of HerMES (far-IR). The orange shaded region is the area covered by MIPS 24 μm observations. X-ray and mid-IR AGNs are also marked as green stars and red squares in the plot.

(A color version of this figure is available in the online journal.)

and mid-IR AGNs. The angular distribution of sources and the coverage of different observations are plotted in Figure 1.

2.5. Star Formation Rate

In this section, we discuss the methods we used to estimate the SFRs with the SPIRE 250 μm observations.

Extrapolation of total IR luminosities (L_{IR}, defined as the integrated luminosity in the 8–1000 μm range) from monochromatic fluxes in the near- to mid-IR wavelengths using templates of infrared spectral energy distributions (SEDs) of local star-forming galaxies (e.g., Chary & Elbaz 2001, CE01 hereafter) has been adopted by a number of previous works to estimate the SFR of galaxies. However, it is also shown that AGNs have significant emission at near- to mid-IR wavelengths (e.g., Daddi et al. 2007; Mullaney et al. 2011), which poses challenges in obtaining reliable estimates of the SFR using mid-IR data.

By contrast, far-IR observations have been shown to suffer minimum contamination from AGNs (e.g., Netzer et al. 2007; Hatziminaoglou et al. 2010; Mullaney et al. 2011; Kirkpatrick et al. 2012), which makes far-IR emission a better tracer of the SF-related L_{IR} in an AGN-hosting galaxy sample. However, recent studies have discovered that estimates using only one SPIRE band and templates based on local star-forming galaxies can substantially overestimate L_{IR} for $z < 1.5$ (Elbaz et al. 2010; Nordon et al. 2012) due to the possible lower dust temperature (e.g., Dale & Helou 2002; Pope et al. 2006) that was not accounted for in the local templates. Therefore, in this work, we adopted the composite SED template from Kirkpatrick et al. (2012, hereafter K12). The $z \sim 1$ K12 template is derived from the *Spitzer* and *Herschel* observations of a sample of star-forming galaxies at $0.4 < z < 1.47$, which is comparable to the redshift range of our sample. From the photometric observations available in both K12 and our sample, we have determined that the distributions of the ratio between the observed 250 μm flux

(S_{250}) and 24 μm flux (S_{24}) in both samples are similar. We found that ~96% of the star-forming galaxies in our sample have S_{250}/S_{24} that lies within the 2σ range (0.34 dex, adopted from Table 3 in K12) of the K12 template S_{250}/S_{24} distribution derived in the redshift range of our sample. This shows that the K12 template can describe the far-IR to mid-IR color in our sample well, thus we can use this template to estimate the total L_{IR} in our sample.

In principle, the far-IR part of an SED for star-forming galaxies, which comprises the bulk of the SF-related L_{IR}, are dominated by the thermal radiation due to cold and warm dust. Thus, the ratio between the monochromatic far-IR flux and the total L_{IR} of the SED should be very similar for star-forming galaxies with similar dust temperatures. In particular, it has also been shown that the star-forming galaxies with and without strong AGNs have similar cold dust temperature (Kirkpatrick et al. 2012). Recent studies using *Herschel* observations have also shown that even for AGN host galaxies, the far-IR ($\geqslant 100$ μm) emissions are still dominated by the cold dust component (e.g., Hatziminaoglou et al. 2010; Kirkpatrick et al. 2012). Thus, we can estimate the SF-related L_{IR} for our sample by normalizing the total infrared luminosity of this template (L_{IR}^{T}) using the 250 μm observations. For each source in our sample, we calculated the ratio between the observed S_{250} and the monochromatic flux of the template at the corresponding observed-frame 250 μm (S_{250}^{T}), and derived the total L_{IR} with the following equation:

$$L_{IR} = \frac{S_{250}}{S_{250}^{T}} L_{IR}^{T}. \tag{1}$$

For the K12 template we chose for this work, $L_{IR}^{T} = 4.2 \times 10^{11} L_{\odot}$, which corresponds closely to the median L_{IR} of our sample.

In this work, the L_{IR} was derived by assuming that the S_{250}/L_{IR} in our sample is similar to that of the K12 composite. For a population of star-forming galaxies, the observed dispersion in S_{250}/L_{IR} depends on the variations in their SED shapes. This dispersion also depends on the redshift since the observed S_{250} traces the SED at different rest-frame wavelengths. Thus, the uncertainty in our L_{IR} measurement can be estimated from the variation in the SED shapes between individual galaxies. However, we cannot directly measure the SED shapes for our Boötes sample, because there is only one photometric band of far-IR observations available. Therefore, we took the 39 $z \sim 1$ sources from K12, and selected a sub-sample of 25 SF-dominated (with mid-IR AGN fraction less than 10%, see K12 for the details in mid-IR spectral decomposition), far-IR-detected (with at least two bands of SPIRE photometry) sources. This sub-sample spans a redshift range of $0.47 < z < 1.24$ and has at least five photometric data points from 24 to 500 μm; thus, it can be used to estimate the dispersion of S_{250}/L_{IR} due to the variation in SEDs for a population of star-forming galaxies.

We first estimated L_{IR} and the shape of SED for each source in the K12 sub-sample by taking the available photometry and calculated the corresponding rest-frame monochromatic luminosity (L_{λ}). Combining L_{λ} for each photometric bands, we calculated a best-fitting spline curve, then integrated along the spline curve in the rest-frame 20–300 μm range. For wavelengths beyond the longest wavelength of the spline curve, we used a linear interpolation by assuming that this part of the SED follows a Rayleigh–Jeans distribution. Since this sub-sample from K12 is selected to be SF-dominated and have far-IR constraints with at least two photometric bands, the

best-fitting spline curves can trace the simple shapes of SF-related SEDs at this wavelength range. The integrated 20–300 μm luminosity (L_{20-300}) probes the thermal radiation from warm and cold dust, and represents the bulk of the total 8–1000 μm L_{IR} (e.g., for the K12 template, $L_{20-300} \sim 0.91 L_{IR}$), thus we can use L_{20-300} as a good proxy of L_{IR}. Along the best-fitting spline curves, we calculated the observed-frame 250 μm fluxes at the redshift range of our Boötes sample, $0.25 < z < 0.8$, which corresponds to rest-frame wavelengths from 200 to 140 μm. The S_{250}/L_{20-300} for each source in the K12 sub-sample can therefore be estimated as a function of redshift. For the K12 composite SED, we also calculated the S_{250}/L_{20-300} in $0.25 < z < 0.8$. We compared the S_{250}/L_{20-300} for each source to that of the K12 template at $0.25 < z < 0.8$, and found that the standard deviations in the differences of S_{250}/L_{20-300} between the K12 sources and the K12 template is ~0.17 dex at $z = 0.25$ and ~0.10 dex at $z = 0.8$. This shows that the deviations in far-IR spectral shapes across a representative population of star-forming galaxies are reasonably small, and thus we can confidently estimate the SF-related L_{IR} using Equation (1) from the observed monochromatic 250 μm flux. Even though the dispersion is lower at higher redshift, we conservatively chose 0.17 dex as the uncertainty in our L_{IR} estimation. This is also consistent with the 0.17 dex uncertainty inferred by K12 for the L_{IR}^{T} of the composite template.

As a check, we compared the L_{IR} for star-forming galaxies from our method (L_{IR}^{250}) with the L_{IR} obtained by directly fitting the *Spitzer* MIPS 24 μm flux to the CE01 library (L_{IR}^{24}), which has been shown to be able to robustly estimate L_{IR} for star-forming galaxies out to $z \sim 1$ (Magnelli et al. 2009), and found that the average difference between L_{IR}^{250} and L_{IR}^{24} is ~0.1 dex. However, we note that the difference is much larger for objects with significant AGN contamination (and thus bluer S_{250}/S_{24}), highlighting the need for far-IR data to measure SFR in AGN hosts.

The SFRs for our sample were derived from L_{IR} using the relation from Kennicutt (1998), modified for a Chabrier initial mass function (IMF; Chabrier 2003; Salim et al. 2007):

$$\frac{SFR}{M_{\odot}\ yr^{-1}} = 1.09 \times 10^{-10} \left(\frac{L_{IR}}{L_{\odot}} \right). \tag{2}$$

Figure 2 shows the distribution in redshift and L_{IR} of our sample. The comparison between the photometric and spectroscopic samples, and the comparison between the L_{IR} of AGNs and star-forming galaxies are also shown as the normalized histograms on the side panels. We note that AGNs and star-forming galaxies have similar distributions in L_{IR} and redshift, suggesting that there is no apparent difference in SF properties between the AGN host galaxies and the star-forming galaxies in our sample.

2.6. Black Hole Accretion Rate

The large observed nuclear luminosities in AGNs are direct manifestations of BH growth through mass accretion (see, e.g., Alexander & Hickox 2012). In this work, we calculated the rest-frame 2–10 keV X-ray luminosity (L_X) for direct comparison with other studies. The k-corrections were calculated based on an X-ray spectral index of 1.7 and a galactic gas column density of $N_H \sim 10^{20}$ cm^{-2}. We chose L_X as a proxy to estimate the BHAR:

$$\dot{M}_{BH} = 0.15 \frac{\epsilon}{0.1} \frac{22.4 L_X}{10^{45}\ erg\ s^{-1}}\ M_{\odot}\ yr^{-1}. \tag{3}$$
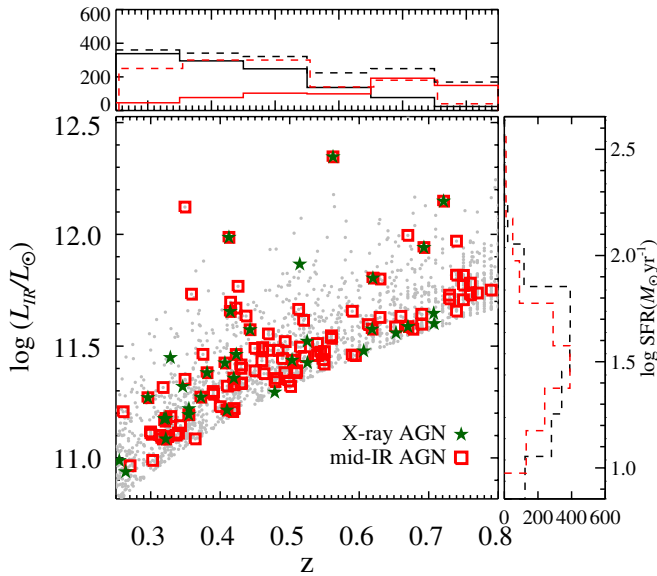
Figure 2. Distribution of redshifts and 8–1000 μm IR luminosities for our sample galaxies detected by both *Herschel* SPIRE 250 μm and *Spitzer* MIPS 24 μm. X-ray AGNs are marked as green stars and mid-IR AGNs are marked as red squares. The histograms in redshift and L_{IR} are also shown in the top and right panels. In the top panel, we show the different redshift distributions of the sources with only photometric redshifts (solid red line) and the sources with only spectroscopic redshifts (solid black line). The redshift distributions of AGNs (red dashed line, normalized to scale) and star-forming galaxies are also shown. In the right panel, we show that AGNs (red dashed line) and star-forming galaxies (black dashed line) have similar distributions in L_{IR} (the histogram of AGNs is normalized to scale). These distributions show that the galaxies with identified AGNs in our sample have distributions in redshift and L_{IR} similar to those of star-forming galaxies.

(A color version of this figure is available in the online journal.)

For simplicity, $\dot{M}_{BH}$ in Equation (3) is derived from L_X with a constant bolometric correction factor of 22.4 (the mean bolometric correction factor from Vasudevan & Fabian 2007, which is based on a sample of local, $L_X = 10^{41-46}$ erg s^{-1}, AGNs.) Here, ϵ is the mass–energy conversion efficiency (we used a typical value $\epsilon \sim 0.1$; see Marconi et al. 2004). In the following paragraphs, we describe the methods we used to calculate the average L_X for all of the star-forming galaxies in our sample.

2.6.1. Mid-IR AGNs

Since some of the actively accreting AGNs are not detected in X-rays due to obscuration, it is important to take them into account when calculating the average SMBH accretion rate for a population of galaxies. In particular, the X-ray stacking analysis in Hickox et al. (2009) shows that mid-IR AGNs without direct X-ray detections have higher average X-ray luminosity and harder X-ray spectra than those of star-forming galaxies at similar redshifts. We therefore assumed that the mid-IR AGNs without X-ray detections are faint in observed X-rays because of obscuration. Since both L_X and the rest-frame 4.5 μm flux density ($L_{4.5}$) can be used to derive the bolometric AGN luminosity with a choice of bolometric correction factors, we first estimated $L_{4.5}$ for the mid-IR AGNs by interpolating the fluxes detected in all four IRAC bands. We next derived an empirical relation between $L_{4.5}$ and L_X for all of the 163 AGNs that are identified by IRAC color–color cuts and are also X-ray detected in the redshift range of $0.25 < z < 0.8$. We found that the median $L_{4.5}/L_X$ for these AGNs is 4.59, or, $L_{4.5} = 4.59L_X$.

From the distribution of $\log(L_{4.5}/L_X)$, we also derived an uncertainty of ~ 0.37 dex in this ratio by fitting a normal distribution to it. We then estimated the L_X from $L_{4.5}$ for the 74 mid-IR AGNs without X-ray detection in our main sample using this empirically derived relation. For convenience, we denote the X-ray luminosity derived from this empirical relation as L_X^{IRAGN}.

2.6.2. X-Ray Stacking of Star-forming Galaxies

Our goal is to study the average BHAR in star-forming galaxies over a range of SFR. We derived the SFR using Equation (2) and divided the galaxies in our sample into bins of SFR with approximately equal size, with the number of galaxies in each bin being at least 5σ above the Poisson noise. To estimate the average X-ray luminosity for all of the star-forming galaxies, we used an X-ray stacking analysis to account for sources not individually detected in X-rays. We defined the stacked X-ray counts as the average number of background-subtracted photons detected within the 90% PSF energy encircled radius at 1.5 keV, r_{90}, where $r_{90} = 1'' + 10''(\theta/10')^2$. Here, θ is the off-axis angle from the *Chandra* optical axis.[12] We adopted background surface brightnesses of 3.0 and 5.0 counts s^{-1} deg^{-2} for the 0.5–2 keV and 2–7 keV bands, based on the estimates of the diffuse background (Hickox et al. 2007). We converted count rates (counts s^{-1}) to flux (erg cm^{-2} s^{-1}) using the conversion factors 6.0×10^{-12} erg cm^{-2} count^{-1} in the 0.5–2 keV band and 1.9×10^{-11} erg cm^{-2} count^{-1} in the 2–7 keV band. The error in the flux can be directly estimated from the error in count rates, which can be calculated using an approximation: $\sigma_X = \sqrt{X + 0.75} + 1$, where X is the number of counts (Gehrels 1986). To estimate the average X-ray stacking luminosity from the X-ray flux, we assumed that all galaxies in each bin of SFR reside at the average luminosity distance for the galaxies in that bin. The uncertainty of the stacked X-ray luminosity can be derived from the combination of errors in the flux and the average luminosity distance. More details of the stacking procedure are described in Section 5.1 of Hickox et al. (2007).

2.6.3. Average X-Ray Luminosity

Combining the contributions of X-ray and mid-IR identified AGNs as well as undetected sources, the average L_X for star-forming galaxies can now be calculated in each bin of SFR:

$$\langle L_X \rangle = \left[\sum_{i=1}^{N_{XAGN}} \left(L_X^{XAGN} \right)_i + \sum_{i=1}^{N_{IRAGN}} \left(L_X^{IRAGN} \right)_i + N_{SFG} L_X^{stacking} \right]$$
$$\times \left[N_{XAGN} + N_{IRAGN} + N_{SFG} \right]^{-1}. \quad (4)$$

Here, N_{XAGN}, N_{IRAGN}, and N_{SFG} are the total numbers of X-ray identified AGNs, mid-IR identified AGNs without direct X-ray detections, and star-forming galaxies without identified AGNs, respectively. L_X^{XAGN} and L_X^{IRAGN} are the X-ray luminosities for individual X-ray AGNs and the mid-IR AGNs, and $L_X^{stacking}$ is the average X-ray luminosity from the stacking analysis for all star-forming galaxies without direct AGN detections in each bin.

We estimated our errors by propagating the observed uncertainties for L_X^{XAGN}, and the uncertainties for L_X^{IRAGN} and $L_X^{stacking}$ estimated in Sections 2.6.1 and 2.6.2 with a bootstrap method.

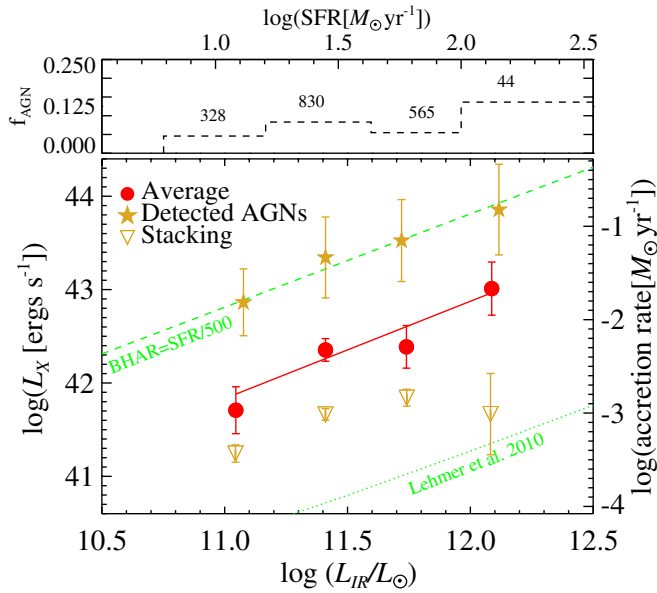[12] *Chandra* Proposers's Observatory Guide (POG), available at http://cxc.harvard.edu/proposer/POG.

Figure 3. SFR–BHAR relation, calculated from the 8–1000 μm L_{IR} and the 2–10 keV L_X with Equations (2) and (3) for the entire 250 μm sample of 1767 galaxies (red circles). The X-ray stacking luminosity for the X-ray non-detections are shown as downward triangles and the X-ray/IRAC-selected AGNs are shown as stars. The sources are binned in approximately equal size SFR bins, with the vertical bars showing the errors from bootstrap re-sampling in each bin. The data points are plotted on the average L_{IR} of each bin. The dashed green line on the top is $\dot{M}_{BH}$ = SFR/500 and the dotted green line in the bottom is the Lehmer et al. (2010) SFR–L_X relation. In the top panel, we also present the AGN detection fraction (f_{AGN}) with the total number of galaxies in each bin. The width of each bin in the histogram covers the SFR range in the bin. This figure shows that the *average* BHAR is strongly correlated with the SFR in all rapidly star-forming galaxies.

(A color version of this figure is available in the online journal.)

The uncertainties in L_{IR} were also taken into our bootstrap analysis. In each bootstrapping sub-sample, we first randomly re-sampled our sources with replacements, then replaced the original L_{IR} for each source using a random normal error with an 1σ value of 0.17 dex. We then re-binned the random sample using the same bins. For each bin, we recalculated the stacked $L_X^{stacking}$ and the uncertainties for the sources that were not identified as AGNs, then replaced the L_X for every detected AGN in the bin with a new L_X within the normal error of the original AGN L_X. Finally, we recalculated the $\langle L_X \rangle$ and the average L_{IR} for each bin. We repeated the bootstrapping 5000 times, at which the variances in $\langle L_X \rangle$ and L_{IR} converge to finite values. The results are shown in Figures 3 and 4 and are discussed in the next section.

3. RESULTS

In this section, we discuss the correlation between the average BHAR and SFR in star-forming galaxies. We divided the galaxies in our sample into bins of SFR, and calculated the *average* BHAR in each bin, yielding an approximately linear correlation between the L_{IR} and the average X-ray luminosity.

3.1. The SFR–BHAR Correlation

Using Equation (4), we can calculate the average L_X in each bin of SFR. However, it is well known that high-mass and low-mass X-ray binaries (HMXBs and LMXBs) can also generate X-ray luminosity that is correlated with SFR (e.g., Grimm et al. 2003; Ranalli et al. 2003; Gilfanov et al. 2004;
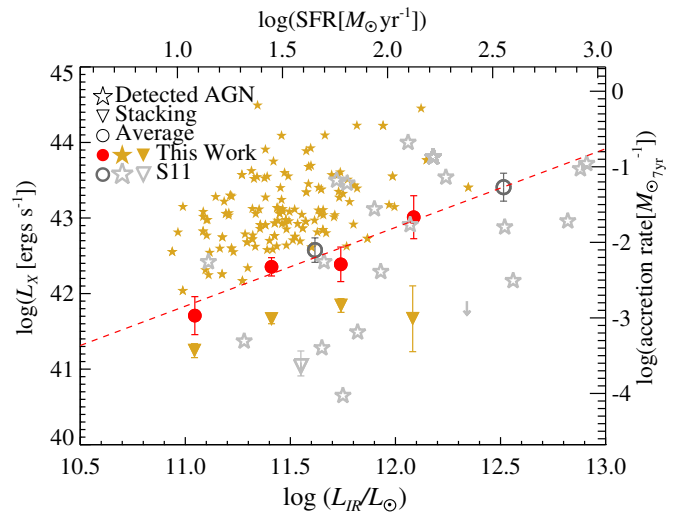

Figure 4. Comparison of our result from Figure 3 (filled symbols) to the SPIRE-selected, $z \sim 1$ sample in the CDF-N field (Symeonidis et al. 2011, open symbols), which is covered by a much deeper, pencil-beam-sized field. The axis, symbols, and the error bars have the same meanings as in Figure 3. The correlation of Equation (5) is shown as the dashed line. This comparison shows that even though the correlation between the L_X and L_{IR} for identified AGNs varies with the depth of the observations, the *average* correlation is consistent.

(A color version of this figure is available in the online journal.)

Lehmer et al. 2010). To accurately estimate the SMBH accretion rate, we calculated the X-ray luminosities related to star-forming processes in each bin of SFR using the equation $L_X^{SF} = \alpha M_\star + \beta$SFR, which is the SFR–$L_X$ relation for HMXBs and LMXBs in Lehmer et al. (2010). In this equation, the stellar mass $M_\star$ is only weakly correlated with SFR in active star-forming galaxies (e.g., SFR > 5 $M_\odot$ yr^{-1}). Thus, for our sample and the Chabrier IMF we adopted, the equation can be re-written into $L_X^{SF} = 10^{26.4}$SFR$^{0.3}$ + $10^{39.3}$SFR (see Equation (3) in Symeonidis et al. 2011, for more details).

In addition, we also tested whether the limited volume of the sample could affect the BHAR–SFR correlation. AGNs with the highest luminosity are rare in this redshift range (and so might not be detected in our survey volume), but may contribute significantly to the $\langle L_X \rangle$ of our sample. We estimated the contribution of these rare, extremely luminous AGNs to the $\langle L_X \rangle$ using the X-ray luminosity function (XLF) from Aird et al. (2010). We note that the AGN XLF was not designed to represent the X-ray luminosity from the sources without direct X-ray observations, thus we first estimated the effect of limited volume on the sources that were identified as AGNs in our sample, i.e., $L_X > 10^{42}$ erg s^{-1}; then, we calculated the effect on the full population by adjusting the result from detected AGNs based on the AGN detection fraction. In detail, at the average redshift range of each SFR bin of our sample, we first calculated the "intrinsic" average AGN luminosity by directly integrating the XLF at $L_X > 10^{42}$ erg s^{-1}. Then, we estimated the "detected" average AGN luminosity by integrating the XLF with a high-end cutoff luminosity, at which the number of the detected AGNs in the volume of each SFR bin is $\leqslant 1$. We found that the difference between the "intrinsic" average AGN luminosity and the "detected" average AGN luminosity is 10%–3% from the first bin to the last bin of SFR in our sample. After the adjustments of the AGN detection fraction in each bin, the corrections on $\langle L_X \rangle$ would become 6.4%, 2.5%, 2.2%, and 2.9%, respectively. These corrections are small and do not make a notable difference to our study of the BHAR–SFR

correlation in the large volume of the Boötes survey region, but might be important when calculating $\langle L_X \rangle$ for a sample with smaller volume. To accurately describe the correlation between the average SMBH growth and SF, we subtracted our $\langle L_X \rangle$ with L_X^{SF}, and also increased our observed $\langle L_X \rangle$ values to account for volume effects as described above. The BHAR were then derived using Equation (3).

We have determined that the average BHAR has a correlation to the SFR in our sample. The results are shown in Figure 3. The average X-ray luminosities, $\langle L_X \rangle$, as determined in Equation (4) are shown as the red circles. The observed L_X for the AGNs identified through X-ray or IRAC observations are shown as the stars, while the stacked L_X for star-forming galaxies without direct X-ray observations are shown as the downward triangles. For comparison, we present the SFR–L_X relation from Lehmer et al. (2010) in Figure 3. We also show the SFR–BHAR correlation corresponding to the local ratio of M_{BH} and M_{bulge} as the green, dashed line on the top of Figure 3. This $\dot{M}_{BH} = $ SFR/500 relation is directly derived from the M_{BH}/M_{Bulge} ratio found in Marconi et al. (2004). Since the average L_X of detected AGNs is subject to the flux limit in the observations, the fact that our data points for detected AGNs sit on the $\dot{M}_{BH} = $ SFR/500 relation is only a coincidence.

The relation between L_{IR} and $\langle L_X \rangle$ as shown in Figure 3 can be fitted with a linear relation given by

$$\log(L_X[\mathrm{erg\,s^{-1}}]) = (30.37 \pm 3.80)$$
$$+ (1.05 \pm 0.33)\log(L_{IR}/L_\odot), \quad (5)$$

which is calculated using the nonlinear least-squares fitting program MPFIT in IDL (Markwardt 2009). The uncertainties in the averages are estimated using bootstrap re-sampling in each bin. The reduced χ^2 of this fitting is 0.99. An equation correlating SFR and BHAR can immediately be derived using Equations (2), (3), and (5):

$$(\mathrm{BHAR}/M_\odot\,\mathrm{yr^{-1}}) = 10^{(-3.72 \pm 0.51)} \left(\frac{\mathrm{SFR}}{M_\odot\,\mathrm{yr^{-1}}} \right)^{(1.05 \pm 0.33)}.$$
$$(6)$$

For an SFR of 100 $M_\odot$ yr^{-1}, this corresponds to a ratio of BHAR to SFR of $\log(\mathrm{BHAR/SFR}) \sim -3.6 \pm 0.2$, where the error is derived from calculating this ratio in each bootstrapping sub-sample when deriving Equation (5).

We also calculated the same correlation using only the sample with spectroscopic redshifts. In this calculation, we adopted the sampling weight w_i to account for the spectroscopic redshift completeness of the AGES sample. The sampling weight is the combination of the sparse sampling weight that accounts for the random target selection incompleteness, the target assignment weight that addresses the fiber-allocation selection, and the redshift weight that accounts for the unsuccessful redshift measurement. The details of the sampling weight can be found in Section 3.1 of Hickox et al. (2009) and Kochanek et al. (2012). Using the same methods, the SFR–BHAR relation for the AGES galaxies with only spectroscopic redshifts can be written as

$$\log(L_X[\mathrm{erg\,s^{-1}}]) = (29.39 \pm 4.72)$$
$$+ (1.14 \pm 0.41)\log(L_{IR}/L_\odot). \quad (7)$$

Here, the power-law index is only higher by ~ 0.1 compared to Equation (5), which is still consistent with the result from our main sample. Since photometric redshift measurements are not

subject to the choices of sampling weights as the spectroscopic sample, we chose the result from Equations (5) and (6) as our primary conclusion in this work.

In Figure 3, we noticed that our stacked L_X is at least ~ 0.7 dex higher than the Lehmer et al. (2010) L_X^{SF} in the first three bins, suggesting that the L_X contribution from SF in our stacked X-ray luminosity is less than $\sim 20\%$ in these bins. For the bin with the highest SFR, the stacked X-ray luminosity is still higher than L_X^{SF} by a factor of two. This shows that while the galaxies we stacked were not identified as AGNs using the common X-AGN selection criterion of $L_X > 10^{42}$ erg s^{-1} or the IRAC color–color selection method, a significant fraction of the average L_X for these star-forming galaxies arises from SMBH accretions. We stress that the $\langle L_X \rangle$ used in our primary analysis is the average L_X due to SMBH accretion only, which was determined by subtracting the expected SF contribution. We note that in an X-ray stacking study in the same Boötes survey region, Watson et al. (2009) concluded that the spectroscopically selected late-type galaxies have their X-ray luminosities dominated by HMXBs. However, the sample in Watson et al. (2009) are galaxies with lower SFRs at lower redshifts. The stacked L_X in the lowest SFR bin in our work is still in agreement with their sample at comparable SFR. Using our methods, deeper far-IR observations would be required to probe the more moderate SFR galaxies studied by Watson et al. (2009).

3.2. Effects of Flux Limit

We note that there might be observational bias in the BHAR-to-SFR correlation in our sample due to the flux limits. The limited flux would cause galaxies with high SFR to be preferentially found at higher redshift. This bias translates into the different average redshift in each bin ($\langle z \rangle = 0.31, 0.46, 0.67, 0.68$ in the four bins of SFR, from low to high.) Studies of redshift evolution of SFR density (e.g., Hopkins & Beacom 2006; Rodighiero et al. 2010) and BHAR density (e.g., Silverman et al. 2009; Aird et al. 2010) suggest that the SFR and BHAR densities are higher at higher redshift (up to $z \sim 2$). Thus, when dividing galaxies into bins of SFR in a flux-limited sample, even if the L_X and L_{IR} are completely uncorrelated in individual galaxies, the redshift evolutions of the XLF and the infrared luminosity function (IRLF) would naturally yield an L_X–L_{IR} relation.

To account for the selection bias due to this effect and to test whether the redshift coevolution of the SFR density and the BHAR density is the dominant factor driving the L_X–L_{IR} correlation observed in this work, we examined the sample by directly computing the effect of the redshift evolution of the X-ray luminosity density (XLD; e.g., Aird et al. 2010, A10 hereafter). In principle, if there is no BHAR–SFR correlation in individual galaxies, then the observed difference of the $\langle L_X \rangle$ between the bins with the lowest and the highest SFR should be consistent with the pure redshift evolution of the XLD. We found that in our sample, the pure redshift evolution of the A10 XLD in the range of the average redshifts in our bins would translate into a difference in $\langle L_X \rangle$ of 0.47 dex.

To address this issue more carefully, we also created a "mock" catalog of galaxies, in which redshift distributions similar to our sample were generated. We generated IR luminosities for the galaxies in the mock catalog based on the IRLF from Rodighiero et al. (2010). Based on the different normalizations of this IRLF and the XLF from A10, we only assigned X-ray luminosities to a fraction of the mock galaxies according to the XLF from A10. For the rest of the galaxies, we assumed their X-ray luminosities to be zero. Since the IR luminosity distribution and X-ray

luminosity distribution were derived independently, there is no intrinsic correlation between L_X and L_{IR} in our mock catalog. To test the effects of the redshift evolution in XLF and the possible Malmquist bias, we took the flux limits in X-ray and far-IR of our sample and applied them to the mock catalog, then repeated the calculations described in Section 3.1 to obtain $\langle L_X \rangle$ in bins of SFR. We found a weak correlation between L_{IR} and $\langle L_X \rangle$ in our mock catalog, $\log L_X = 37.45 \pm 1.93 + (0.30 \pm 0.17) \log L_{IR}$. The difference in $\langle L_X \rangle$ between the bins with the highest and the lowest SFR is 0.38 dex, which is similar to the effect of pure XLD evolution we estimated in the previous paragraph. In Equation (5), we found that there is at least 1.31 dex difference in the $\langle L_X \rangle$ of the bins with the lowest and the highest SFR in our sample, indicating that most, if not all, of our observed trend is due to the intrinsic correlation between SFR and BHAR.

3.3. Comparison to Previous Studies

To examine whether the average SFR–BHAR correlation is subject to the limiting fluxes of the observations, we compared our result with the sample of *Herschel*-selected star-forming galaxies in the pencil-beam Chandra Deep Field-North (CDF-N; Symeonidis et al. 2011) at redshift $z \sim 1$. From Table 2 in Symeonidis et al. (2011), we selected the galaxies with hard (2–10 keV) X-ray detections and L_{IR} larger than $10^{11} L_\odot$, in which the average X-ray luminosity for the X-ray non-detected galaxies have been estimated. For these luminous infrared galaxies (LIRGs) and ultraluminous infrared galaxies (ULIRGs), we calculated the average luminosity and the error in the 2–10 keV X-ray using a bootstrap re-sampling method similar to what we used for the Boötes data. Since there is no stacking signal in the ULIRG bin, we used the lower limit ($L_X = 0$) for the X-ray non-detected sources in that bin to estimate the error in $\langle L_X \rangle$ conservatively. We also estimated the effects of the limited volume in this field using a similar approach described in the second paragraph of Section 3.1, and found that the possible non-detections of the rare, high-luminosity AGNs might decrease the $\langle L_X \rangle$ by $\sim 26\%$ in the LIRG bin, and $\sim 7\%$ in the ULIRG bin. For the $\langle L_X \rangle$ in both our sample and the Symeonidis et al. (2011) sample, we subtracted by L_X^{SF} and made adjustments to account for the bias due to limited volume. A comparison of the results are displayed in Figure 4, which shows that in samples of star-forming galaxies with different X-ray flux limits, even though the average L_X for the detected AGNs are different (so are the average L_X for the galaxies without direct X-ray detections), the *average* L_X to L_{IR} relations are consistent.

4. DISCUSSION

In the previous section, we presented the SFR-to-average BHAR correlation we found for the far-IR-selected star-forming galaxies. From our X-ray stacking analysis, we found that the average L_X of star-forming galaxies in our sample has an X-ray luminosity dominated by SMBH accretion instead of SF. This implies that BH growth is not limited to the detected AGNs only. Recent studies also argue for a picture that departs from a simple duty cycle scenario for SMBH accretion. In the duty cycle scenario, SMBHs accrete most of their mass during short episodes of accretion near the Eddington limit, and are relatively quiescent otherwise. In comparison, Hopkins & Hernquist (2009b), Aird et al. (2012), and Bongiorno et al. (2013) show that a substantial population of AGNs spend most of their lifetime accreting at lower Eddington ratio. Hence, the SMBH growth during the lower Eddington ratio state cannot be

neglected. In this vein, and considering that AGNs may vary by over five orders of magnitude in Eddington ratio on a timescale much shorter than that of galactic SF (e.g., Hickox et al. 2009; Hopkins & Hernquist 2009b; Novak et al. 2011; Aird et al. 2012; Bongiorno et al. 2013), we argue that the *average* BHAR is a more appropriate tracer to study the correlation to the SFR, since the detected AGNs are only a small fraction of accreting SMBHs residing at the higher end of the Eddington ratio distribution. We have found evidence consistent with a universal BHAR–SFR correlation (Equations (5) and (6)). This result is consistent with a simple picture in which the BHAR–SFR link exists in star-forming galaxies over a wide range of SFR. We argue that the discrepancy between our result and the scenario where AGNs and SF are only linked in the most rapidly growing systems can be attributed to the timescale difference between the variability of AGN accretion efficiency and SF (Mullaney et al. 2012a, Hickox et al. 2013).

We note that the observed ratio between BHAR and SFR in our work is lower than the observed BH mass (M_{BH}) to galaxy bulge mass (M_{Bulge}) ratio for local galaxies. Other studies have also obtained BHAR-to-SFR ratios consistent with the values observed here (Rafferty et al. 2011; Mullaney et al. 2012a). Different arguments have been proposed to explain the low BHAR-to-SFR ratio. One is that the SF in disk galaxies tends to concentrate in their disks, which leads to a BHAR to galaxy-wide SFR ratio lower than that inferred by the observed M_{BH} and M_{Bulge} (e.g., Jahnke et al. 2009; Cisternas et al. 2011a, 2011b; Rafferty et al. 2011). In addition, the average BHAR might be underestimated due to non-detections of a substantial population of heavily obscured AGNs, which can be responsible for as much as 50% of SMBH growth (e.g., Gilli et al. 2007; Treister et al. 2009; Mullaney et al. 2012a).

In summary, we studied the average BHAR for a sample of star-forming galaxies with SFR measurements without contamination from AGNs using *Herschel*. We used AGNs selected at X-ray and mid-IR wavelengths to ensure that our BHAR is not biased by AGN obscuration, and employed an X-ray stacking analysis to measure SMBH accretion for star-forming galaxies without direct X-ray detections. We obtained an almost linear relation between the average BHAR and SFR of $\log BHAR = (-3.72 \pm 0.52) + (1.05 \pm 0.33) \log SFR$, and determined that this relation also holds for deeper, narrower observations, suggesting that the average BHAR-to-SFR correlation is a universal consequence of the coevolution between SMBHs and galaxies. The next step to understanding the SFR-to-BHAR correlation in different populations of galaxies requires information on the *distribution* of AGN X-ray luminosity as a function of SFR, which will only be possible with a wide, deep X-ray survey.

REFERENCES

Aird, J., Coil, A. L., Moustakas, J., et al. 2012, ApJ, 746, 90
Aird, J., Nandra, K., Laird, E. S., et al. 2010, MNRAS, 401, 2531
Alexander, D. M., Chary, R., Pope, A., et al. 2008, ApJ, 687, 835
Alexander, D. M., & Hickox, R. C. 2012, NewAR, 56, 93
Ashby, M. L. N., Stern, D., Brodwin, M., et al. 2009, ApJ, 701, 428
Assef, R. J., Kochanek, C. S., Brodwin, M., et al. 2010, ApJ, 713, 970
Bongiorno, A., Merloni, A., Brusa, M., et al. 2013, MNRAS, 427, 3103
Brodwin, M., Brown, M. J. I., Ashby, M. L. N., et al. 2006, ApJ, 651, 791
Chabrier, G. 2003, PASP, 115, 763
Chapin, E. L., Chapman, S. C., Coppin, K. E., et al. 2011, MNRAS, 411, 505
Chary, R., & Elbaz, D. 2001, ApJ, 556, 562
Ciotti, L., Ostriker, J. P., & Proga, D. 2010, ApJ, 717, 708
Cisternas, M., Jahnke, K., Bongiorno, A., et al. 2011a, ApJL, 741, L11
Cisternas, M., Jahnke, K., Inskip, K. J., et al. 2011b, ApJ, 726, 57
Daddi, E., Dickinson, M., Morrison, G., et al. 2007, ApJ, 670, 156
Dale, D. A., & Helou, G. 2002, ApJ, 576, 159
Dekel, A., Birnboim, Y., Engel, G., et al. 2009, Natur, 457, 451
Donley, J. L., Rieke, G. H., Pérez-González, P. G., Rigby, J. R., & Alonso-Herrero, A. 2007, ApJ, 660, 167
Eisenhardt, P. R., Stern, D., Brodwin, M., et al. 2004, ApJS, 154, 48
Elbaz, D., Dickinson, M., Hwang, H. S., et al. 2011, A&A, 533, A119
Elbaz, D., Hwang, H. S., Magnelli, B., et al. 2010, A&A, 518, L29
Ferrarese, L., & Merritt, D. 2000, ApJL, 539, L9
Gebhardt, K., Bender, R., Bower, G., et al. 2000, ApJL, 539, L13
Gehrels, N. 1986, ApJ, 303, 336
Genzel, R., Tacconi, L. J., Gracia-Carpio, J., et al. 2010, MNRAS, 407, 2091
Gilfanov, M., Grimm, H.-J., & Sunyaev, R. 2004, MNRAS, 347, L57
Gilli, R., Comastri, A., & Hasinger, G. 2007, A&A, 463, 79
Gorjian, V., Brodwin, M., Kochanek, C. S., et al. 2008, ApJ, 679, 1040
Goulding, A. D., & Alexander, D. M. 2009, MNRAS, 398, 1165
Griffin, M. J., Abergel, A., Abreu, A., et al. 2010, A&A, 518, L3
Grimm, H.-J., Gilfanov, M., & Sunyaev, R. 2003, MNRAS, 339, 793
Harrison, C. M., Alexander, D. M., Mullaney, J. R., et al. 2012, ApJL, 760, L15
Hatziminaoglou, E., Omont, A., Stevens, J. A., et al. 2010, A&A, 518, L33
Hickox, R. C., Jones, C., Forman, W. R., et al. 2007, ApJ, 671, 1365
Hickox, R. C., Jones, C., Forman, W. R., et al. 2009, ApJ, 696, 891
Hickox, R. C., Mullaney, J. R., Alexander, D. M., et al. 2013, ApJ, submitted (arXiv:1306.3218)
Hickox, R. C., Wardlow, J. L., Smail, I., et al. 2012, MNRAS, 421, 284
Hopkins, A. M., & Beacom, J. F. 2006, ApJ, 651, 142
Hopkins, P. F., & Hernquist, L. 2009a, ApJ, 694, 599
Hopkins, P. F., & Hernquist, L. 2009b, ApJ, 698, 1550
Jahnke, K., Bongiorno, A., Brusa, M., et al. 2009, ApJL, 706, L215
Jannuzi, B. T., & Dey, A. 1999, in ASP Conf. Ser. 191, Photometric Redshifts and the Detection of High Redshift Galaxies, ed. R. Weymann, L. Storrie-Lombardi, M. Sawicki, & R. Brunner (San Francisco, CA: ASP), 111
Kauffmann, G., Heckman, T. M., Tremonti, C., et al. 2003, MNRAS, 346, 1055
Kawakatu, N., & Wada, K. 2008, ApJ, 681, 73
Keel, W. C., Chojnowski, S. D., Bennert, V. N., et al. 2012a, MNRAS, 420, 878
Keel, W. C., Lintott, C. J., Schawinski, K., et al. 2012b, AJ, 144, 66
Kennicutt, R. C. 1998, ARA&A, 36, 189
Kenter, A., Murray, S. S., Forman, W. R., et al. 2005, ApJS, 161, 9
Kirkpatrick, A., Pope, A., Alexander, D. M., et al. 2012, ApJ, 759, 139
Kochanek, C. S., Eisenstein, D. J., Cool, R. J., et al. 2012, ApJS, 200, 8
Lacy, M., Storrie-Lombardi, L. J., Sajina, A., et al. 2004, ApJS, 154, 166
Lehmer, B. D., Alexander, D. M., Bauer, F. E., et al. 2010, ApJ, 724, 559
Lutz, D., Mainieri, V., Rafferty, D., et al. 2010, ApJ, 712, 1287
Lutz, D., Sturm, E., Tacconi, L. J., et al. 2008, ApJ, 684, 853
Magnelli, B., Elbaz, D., Chary, R. R., et al. 2009, A&A, 496, 57
Magorrian, J., Tremaine, S., Richstone, D., et al. 1998, AJ, 115, 2285
Marconi, A., Risaliti, G., Gilli, R., et al. 2004, MNRAS, 351, 169
Markwardt, C. B. 2009, in ASP Conf. Ser. 411, Astronomical Data Analysis Software and Systems XVIII, ed. D. A. Bohlender, D. Durand, & P. Dowler (San Francisco, CA: ASP), 251
Mor, R., Netzer, H., Trakhtenbrot, B., Shemmer, O., & Lira, P. 2012, ApJL, 749, L25
Mullaney, J. R., Alexander, D. M., Goulding, A. D., & Hickox, R. C. 2011, MNRAS, 414, 1082
Mullaney, J. R., Daddi, E., Béthermin, M., et al. 2012a, ApJ, 753, 6
Mullaney, J. R., Pannella, M., Daddi, E., et al. 2012b, MNRAS, 419, 95
Murray, S. S., Kenter, A., Forman, W. R., et al. 2005, ApJS, 161, 1
Netzer, H., Lutz, D., Schweitzer, M., et al. 2007, ApJ, 666, 12
Nobukawa, M., Ryu, S. G., Tsuru, T. G., & Koyama, K. 2011, ApJL, 739, L52
Nordon, R., Lutz, D., Genzel, R., et al. 2012, ApJ, 745, 182
Novak, G. S., Ostriker, J. P., & Ciotti, L. 2011, ApJ, 737, 26
Oliver, S. J., Bock, J., Altieri, B., et al. 2012, MNRAS, 424, 1614
Ostriker, E. C., McKee, C. F., & Leroy, A. K. 2010, ApJ, 721, 975
Page, M. J., Symeonidis, M., Vieira, J. D., et al. 2012, Natur, 485, 213
Ponti, G., Terrier, R., Goldwurm, A., Belanger, G., & Trap, G. 2010, ApJ, 714, 732
Pope, A., Chary, R.-R., Alexander, D. M., et al. 2008, ApJ, 675, 1171
Pope, A., Scott, D., Dickinson, M., et al. 2006, MNRAS, 370, 1185
Rafferty, D. A., Brandt, W. N., Alexander, D. M., et al. 2011, ApJ, 742, 3
Ranalli, P., Comastri, A., & Setti, G. 2003, A&A, 399, 39
Revnivtsev, M. G., Churazov, E. M., Sazonov, S. Y., et al. 2004, A&A, 425, L49
Rodighiero, G., Vaccari, M., Franceschini, A., et al. 2010, A&A, 515, A8
Rosario, D., Santini, P., Lutz, D., et al. 2012, A&A, 545, A45
Rovilos, E., Comastri, A., Gilli, R., et al. 2012, A&A, 546, A58
Salim, S., Rich, R. M., Charlot, S., et al. 2007, ApJS, 173, 267
Schawinski, K., Urry, C. M., Virani, S., et al. 2010, ApJ, 711, 284
Serjeant, S., Bertoldi, F., Blain, A. W., et al. 2010, A&A, 518, L7
Serjeant, S., & Hatziminaoglou, E. 2009, MNRAS, 397, 265
Shao, L., Lutz, D., Nordon, R., et al. 2010, A&A, 518, L26
Silverman, J. D., Lamareille, F., Maier, C., et al. 2009, ApJ, 696, 396
Stern, D., Eisenhardt, P., Gorjian, V., et al. 2005, ApJ, 631, 163
Symeonidis, M., Georgakakis, A., Seymour, N., et al. 2011, MNRAS, 417, 2239
Treister, E., Urry, C. M., & Virani, S. 2009, ApJ, 696, 110
Vasudevan, R. V., & Fabian, A. C. 2007, MNRAS, 381, 1235
Veilleux, S., Kim, D.-C., Rupke, D. S. N., et al. 2009, ApJ, 701, 587
Watson, C. R., Kochanek, C. S., Forman, W. R., et al. 2009, ApJ, 696, 2206
Wong, T. 2009, ApJ, 705, 650